EPJ Web of Conferences **293**, 00003 (2024) https://doi.org/10.1051/epjconf/202429300003
mm Universe 2023

Cosmology with galaxy clusters: An improved multi-wavelength analysis

G. Aymerich[1,2,*], M. Douspis[1], G. W. Pratt[2], L. Salvati[1], E. Soubrié[1], F. Andrade-Santos[3,4], W. Forman[3], and C. Jones[3]

[1]Institut d'Astrophysique Spatiale, CNRS, Université Paris-Saclay, Bât. 121, 91405 Orsay Cedex, France
[2]AIM, CEA, CNRS, Université Paris-Saclay, Université Paris Diderot, Sorbonne Paris Cité, 91191 Gif-sur-Yvette, France
[3]Center for Astrophysics, Harvard & Smithsonian, 60 Garden Street, Cambridge, MA 02138, USA
[4]Department of Liberal Arts and Sciences, Berklee College of Music, 7 Haviland Street, Boston, MA 02215, USA

Abstract. We provide a new scaling relation using a sample of clusters from a full re-observation by the X-ray Chandra telescope of the Planck ESZ catalogue, and compare it to the results of the Planck collaboration obtained from a smaller sample of XMM-Newton observations. We discuss the expected effects of the change of the scaling relation parameters on the cosmological constraints obtained from the Planck cluster sample, and the remaining steps to obtain final constraints from this new scaling relation.

1 Introduction

A key feature of galaxy clusters is their multi-component nature: they are composed of a dark matter halo, which is the main component of their mass, and of baryonic matter in the form of both hot gas and galaxies. They can therefore be observed through multiple physical processes depending on the wavelength, revealing different properties of the cluster. In optical wavelengths, the member galaxies can be directly observed, and the cluster can be also detected through the gravitational lensing effect on background galaxies. In X-rays, the hot gas emits thermal bremsstrahlung radiation, and in the microwave wavelengths, the hot gas interacts with the cosmic microwave background (CMB) photons through the thermal Sunyaev-Zel'dovich (SZ) effect.

A common method to constrain cosmological parameters with cluster surveys is to compare the observed cluster abundance with the theoretical halo mass function, which predicts halo abundance per unit volume and mass as a function of cosmological parameters. This approach therefore requires knowledge of the cluster masses and redshifts. The mass of a cluster can be estimated through the gravitational lensing effect but this requires a large number of background galaxies to be detected, and therefore long exposure times for every cluster. With cluster catalogs containing several hundreds of objects, this method cannot be applied to each individual cluster. Other observables thus need to be related to the cluster mass, via scaling relations.

*e-mail: gaspard.aymerich@universite-paris-saclay.fr

In the Planck collaboration 2013 and 2015 papers [1, 2], cosmological parameters were constrained using the number counts of SZ-detected clusters. The cluster masses were estimated through a $Y_{SZ} - M_{500}$ scaling relation, calibrated on a subsample of 71 Planck-detected clusters with pre-existing X-ray observations from XMM-Newton. The X-ray data was used to compute the mass of the clusters under an hydrostatic equilibrium hypothesis, and the SZ signal was extracted via a matched multi-frequency filter (MMF) algorithm.
In this work, we use X-ray Chandra observations of the 147 clusters with redshift $z < 0.35$ from the Planck ESZ catalogue [3], to calibrate a new $Y_{SZ} - M_{500}$ scaling relation. This will not only provide a robustness check to the constraints formerly obtained, but also improve on the Planck collaboration approach on two key aspects. The larger calibration sample should provide better statistical constraining power as well as better representativity of the full sample with it being a full re-observation of a SZ-selected sample. While obtaining final cosmological constraints is outside the scope of this work and will be the object of a future publication, we discuss the expected effects of the change of the scaling relation parameters on the cosmological constraints obtained from the Planck cluster sample, and the remaining steps to obtain final constraints from this new scaling relation.
For this work, we use the following cosmological parameters: $\Omega_m = 0.3$, $\Omega_\Lambda = 0.7$, $H_0 = 70\text{km s}^{-1}\text{ Mpc}^{-1}$. Unless explicitely stated, all quantities are given within R_{500}, the radius within which the mean density is 500 times the critical density of the Universe at the cluster redshift.

2 Data and analysis

2.1 Chandra observation of Planck ESZ sample

For our investigation, we use the data set presented in Andrade-Santos et al. 2021 [3], which is derived from X-ray Chandra observations of 147 clusters with redshift z <0.35 from the Planck ESZ catalogue. The sample and data reduction process is fully described in [3], and we refer the reader to this paper for more details. In this section, we compare the sample to the ones used in [1, 2], and briefly summarise the main steps of the data reduction process.

2.1.1 Sample population and comparison with Planck 2013 and 2015

The Planck MMF3 cosmological sample, presented in [4], is composed of all the clusters detected in Planck HFI maps by the MMF3 with a signal-to-noise ratio above 6. It contains 439 clusters and is the sample used to constrain cosmological parameters via MCMC fitting of the number counts in [2]. In order to estimate the masses of the clusters, the Planck collaboration used a scaling relation between the SZ signal and the cluster mass, calibrated on a subsample of 71 clusters with X-ray observations from XMM-Newton [1]. In this work, we use a new calibration sample of 147 clusters from the Planck ESZ catalogue with Chandra X-ray observations.
Figure 1 shows the redshift and mass distribution of the Planck MMF3 cosmological sample, the XMM-Newton calibration sample and the Chandra calibration sample. Compared to the XMM-Newton sample, the Chandra calibration sample has more clusters and extends to lower masses and redshifts. Given the cut at redshift 0.35, the maximum redshift of the Chandra sample is lower than the one of the XMM sample, which has 6 clusters with $0.35 < z < 0.45$.

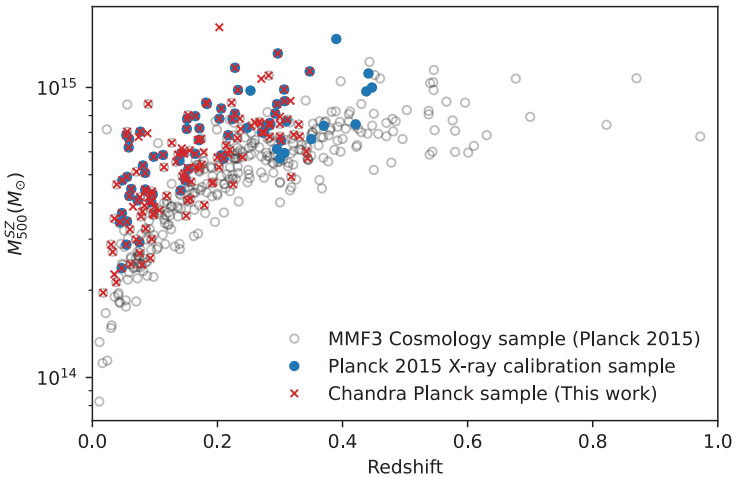

Figure 1. Mass-redshift distribution of the Planck MMF3 cosmological sample, the XMM-Newton calibration sample used by the Planck collaboration and the Chandra calibration used in this work.

2.1.2 Event file processing and density profiles

The full data reduction process from raw event files to profiles is described in [3]. In this section, we briefly summarise the main steps of the data reduction process.
Charge-transfer inefficiency, mirror contamination, CCD non-uniformity and time dependence of gain are corrected for during data reduction. High background periods are removed, and blank sky background and readout artefacts are substracted from the signal. Point sources and extended substructures are masked before analysing the cluster emission.
Surface brightness profiles are extracted in the 0.7-2keV band, where signal-to-noise ratio is maximal, in concentric annuli around the X-ray emission peak. Spectra are extracted in larger concentric annuli, and fitted with an absorbed single temperature thermal model. The projected temperature profiles are then fitted with a 3D temperature model to obtain the deprojected temperature profiles. These are then used to compute the emission measure profiles from the surface brightness, which are fitted with the gas density model given by [5].

2.1.3 X-ray mass estimates

In [3], total cluster masses are computed from the gas mass and temperature, using the $Y_X - M_{500}$ scaling relation calibrated in [6]:

$$M_{500} = E(z)^{-2/5}(5.77 \pm 0.20) \cdot 10^{14}\, h^{1/2}\, M_\odot \left(\frac{Y_X}{3 \cdot 10^{14}\, M_\odot \mathrm{keV}} \right)^{0.57 \pm 0.03} \quad (1)$$

Y_X is defined as the product of M_{gas}, the gas mass inside R_{500}, and T_X^{exc}, the core-excised temperature obtained by fitting a single temperature thermal model on the $0.15R_{500}$ to R_{500} region. It is thus measured within R_{500}, and the mass calculations have to be done following an iterative process described in [7].

2.2 SZ data from Planck

To calibrate the $Y_{SZ} - M_{500}$ scaling relation, we use SZ signal extracted from the Planck DR2 maps, by running a matched multi-frequency filter algorithm, with the X-ray derived positions and sizes. The MMF algorithm extracts the Y_{SZ} signal from the Planck maps using the universal pressure profile from [8], as well as information on the Planck beam and SZ frequency spectrum. This step was done both in [3] and in this work, using the same X-ray input positions and aperture, but fully independently developped MMF algorithms, allowing for a robustness check of the results. The agreement is excellent when performing a power law fit, with no significant departure from unity in both slope and intercept, as well as very low intrinsic scatter (∼1%).

3 Calibrating the scaling relation

In order to study the effect of the change of calibration sample, we calibrate the $Y_{SZ} - M_{500}$ scaling relation following the Planck collaboration approach described in appendix A of [1]. Since the ESZ sample is signal-to-noise limited, the detected objects will be biased high with respect to the mean close to the signal-to-noise threshold due to the intrinsic scatter of the relation σ_{int}. This effect, commonly known as Malmquist bias, is accounted for following an approach similar to the method presented in [6]. Each individual Y_{SZ} value is corrected by dividing it by the mean bias m at the corresponding signal-to-noise ratio:

$$\begin{aligned} &Y_{SZ}^{corrected} = Y_{SZ}/m \ \text{ with } \ \ln m = \frac{\exp\left(-x^2/2\sigma^2\right)}{\sqrt{\pi/2}\,\mathrm{erfc}\left(-x/\sqrt{2}\sigma\right)}\sigma \\ &\text{where } x = -\log\left(\frac{(S/N)}{(S/N)_{cut}}\right) \ \text{ and } \ \sigma = \sqrt{\ln[((S/N)+1)/(S/N)]^2 + (\ln 10\,\sigma_{int})^2} \end{aligned} \tag{2}$$

The corrected Y_{SZ} values are then used to calibrate the $Y_{SZ} - M_{500}^{Y_X}$ scaling relation, using a Markov Chain Monte Carlo (MCMC) approach, using the emcee sampler [9]. Other linear regression methods (LinMix [10] and BCES [11]) were tried, with no significant difference in the results. Figure 3 shows the scaling relation obtained with the emcee sampler, and compares it with the one obtained by the Planck collaboration with XMM Newton calibration sample. For comparison, the pivot points were chosen to be the same in this work as in the Planck collaboration work, i.e. $M_{500}^{Y_X} = 6 \cdot 10^{14} M_\odot$ and $Y_{SZ} = 10^{-4}\mathrm{Mpc}^2$.
This scaling relation is not final: the $Y_{SZ} - M_{500}^{Y_X}$ relation needs to be combined with the $M_{500}^{Y_X} - M_{500}$ relation to obtain the $Y_{SZ} - M_{500}$ relation. The $M_{500}^{Y_X} - M_{500}$ relation has the following form, with σ_A and σ_α the uncertainties in the normalisation and slope of the $Y_X - M_{500}$ relation [1]:

$$M_{500}^{Y_X} = 10^{\pm\sigma_A/\alpha}[(1-b)M_{500}]^{1\pm\sigma_\alpha/\alpha} \tag{3}$$

Combining the two relations, we obtain the following $Y_{SZ} - M_{500}$ relation:

$$E^{-2/3}(z)\frac{D_A^2\, Y_{SZ}}{10^{-4}\mathrm{Mpc}^2} = 10^{-0.29\pm0.01}\left(\frac{(1-b)M_{500}}{6\cdot 10^{14} M_\odot}\right)^{1.71\pm0.1} \tag{4}$$

Moving from $Y_{SZ} - M_{500}^{Y_X}$ to $Y_{SZ} - M_{500}$, the best fit parameters do not change, but the uncertainties of the $M_{500}^{Y_X} - M_{500}$ relation are propagated, leading to increased uncertainties in the final $Y_{SZ} - M_{500}$ relation. In addition, the scatter around the mean relation is also affected: assuming the scatter around both relations is independent, our final estimate of the scatter is $\sigma_{Y_{SZ}-M_{500}} = 20\%$.

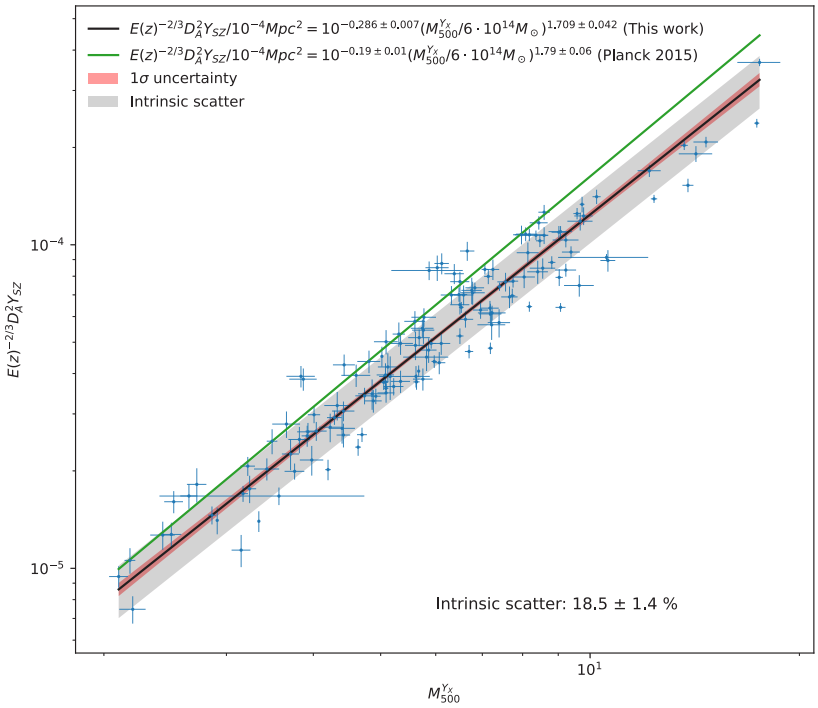

Figure 2. Calibration of the $Y_{SZ} - M_{500}^{Y_X}$ scaling relation. The black line shows the best fit relation obtained in this work, with red contours corresponding to 1σ uncertainties, while the green line shows the best fit relation obtained in [1].

4 Discussion and Conclusion

We calibrated a new $Y_{SZ} - M_{500}$ scaling relation for mass estimation of Planck detected clusters, using Chandra X-ray observations of the 147 clusters with redshift $z < 0.35$ from the Planck ESZ catalogue. We closely followed the method described in appendix A of [1] in order study the effect of changing the calibration sample without introducing additional differences. Table 1 compares the scaling relation obtained in this work to the one obtained by the Planck collaboration. The scaling relations differ in both normalisation and slope.

Table 1. Comparison of the scaling relation parameters and their uncertainties obtained in this work and by the Planck collaboration.

Calibration sample	normalisation	slope	scatter
Chandra (this work)	0.51 ± 0.01	1.71 ± 0.1	20%
XMM-Newton (Planck collab.)	0.65 ± 0.03	1.79 ± 0.08	18%

The lower normalisation obtained in this work is due to the fact that cluster temperatures measured by Chandra are systematically higher than those measured by XMM-Newton, leading to higher masses [12]. Taking the non-unitary slope of the relation into account, the difference of 20% in normalisation is fully consistent with the expected difference in mass of 16% from [12]. The shallower slope can also be explained by the instrumental differences,

as the difference in temperature and therefore mass is larger at larger temperatures/masses. This leads to the difference of mass between the least and most massive clusters to be greater in the Chandra sample than in the XMM-Newton sample, and therefore to a shallower slope. We note that the slope obtained in this work is closer to the expected self-similar value of 5/3.

In terms of uncertainties and scatter, the scaling relations are similar. While this is expected for scatter, one would expect that a scaling relation calibrated on a larger sample would have smaller uncertainties. While this holds for the $Y_{SZ} - M_{500}^{Y_X}$ relations, it is no longer true for the final $Y_{SZ} - M_{500}$ relations, for which the uncertainty on the slope is larger in this work. This can be explained by the difference in the $M_{500}^{Y_X} - M_{500}$ relation, which is different for the XMM-Newton and Chandra samples since the X-ray data comes from different instruments. In this work, equation 1 is used for the Chandra sample, while the Planck collaboration used the $Y_X - M_{500}$ relation from [8] for the XMM-Newton sample. The latter has lower uncertainties, which when propagated, lead to similar uncertainties in the final $Y_{SZ} - M_{500}$ relation, even if the sample used in this work is larger.

While obtaining cosmological constraints is outside the scope of this work and will be presented in a future analysis, we can discuss the expected effect of the change of scaling relation parameters on the cosmological constraints obtained from the Planck cluster sample. As detailed in the previous paragraph, the scaling relation obtained in this work leads to overall heavier clusters, and to a greater difference of mass between light and heavy clusters. The first effect is fully degenerate with a change of mass bias, which has been shown to shift the $\Omega_m - \sigma_8$ constraints in the $S_8 = \sigma_8 \sqrt{\Omega_m/0.3}$ direction in [2]. The second effect will lead to a shift of constraints towards higher σ_8 values, as the number of very massive clusters is increased. These expected predictions were verified by pulling cosmological constraints while letting the scaling relation parameters vary one at a time.

One of the main steps left before obtaining final cosmological constraints is the re-calibration of the mass bias. As the masses obtained from the SZ-signal with the new scaling relation differ from the ones obtained with the XMM-Newton scaling relation, the mass bias needs to be re-calibrated, by comparing the new SZ mass estimates with weak lensing mass estimates. This is expected to reduce the shift of constraints in the S_8 direction due to the difference in scaling relation normalisation, but should not compensate for the change of slope and preference for higher σ_8 values.

References

[1] Planck Collaboration et al., A&A **571**, A20 (2014)
[2] Planck Collaboration et al., A&A **594**, A24 (2016)
[3] F. Andrade-Santos et al., ApJ **914**, 58 (2021)
[4] Planck Collaboration et al., A&A **594**, A27 (2016)
[5] A. Vikhlinin et al., ApJ **640**, 691 (2006)
[6] A. Vikhlinin et al., ApJ **692**, 1033 (2009)
[7] A.V. Kravtsov et al., ApJ **650**, 128 (2006)
[8] M. Arnaud et al., A&A **517**, A92 (2010)
[9] D. Foreman-Mackey et al., Publications of the Astronomical Society of the Pacific **125**, 306 (2013)
[10] B.C. Kelly, ApJ **665**, 1489 (2007)
[11] M.G. Akritas et al., ApJ **470**, 706 (1996)
[12] G. Schellenberger et al., A&A **575**, A30 (2015)